sciendo

Effect of electron beam irradiation on filtering facepiece respirators integrity and filtering efficiency

Dagmara Chmielewska (ID),
Łukasz Werner (ID),
Urszula Gryczka (ID),
Wojciech Migdał (ID)

Abstract. The outbreak of the COVID-19 pandemic has shown that the demand for medical masks and respirators exceeds the current global stockpile of these items, and there is a dire need to increase the production capacity. Considering that ionizing radiation has been used for sterilization of medical products for many years and electron beam (EB) irradiation enables the treatment of huge quantities of disposable medical products in a short time this method should be tested for the mask's decontamination. In this work, three different filtering facepiece respirators (FFRs) were irradiated with electron beams of 12 kGy and 25 kGy. The results confirmed that the decrease in filtration efficiency after irradiation of all respirators results from the elimination of the electric charge from the polypropylene (PP) fibers in the irradiation process. Moreover, the applied doses may affect the thermal stability of PP fabrics, while filtering materials structure and integrity have not changed after irradiation.

D. Chmielewska✉, U. Gryczka, W. Migdał
Institute of Nuclear Chemistry and Technology
Dorodna 16 Str., 03-195 Warsaw, Poland
E-mail: d.chmielewska@ichtj.waw.pl

Ł. Werner
Warsaw University of Technology
Faculty of Chemical and Process Engineering
Warynskiego 1 Str., 00-645 Warsaw, Poland

Introduction

The discussion around transmission routes of the SARS-CoV-2 virus has been accompanying the outbreak of the COVID-19 pandemic. Currently, available research supports the theory that the virus could spread not only by direct contact with the infected person, contaminated surfaces, or fomites but may also spread by airborne transmission [1–3]. Respiratory droplets that may contain virus particles could be generated not only during coughing or sneezing but also are produced during laughing, breathing, or speaking. Moreover, the size of the expiratory particles emitted in each of these activities is different [4]. Larger droplets precipitate quickly on the ground or another surface before drying, but smaller ones may stay longer in the air and become aerosolized particles. Therefore, special safety measures like handwashing, social distancing, and use of personal protective equipment (PPE) like filtering facepiece respirators (FFRs) should be implemented to prevent the SARS-CoV-2 transmission.

The European Standard EN 149:2001 specifies minimum requirements for FFRs. On the basis of the standard three classes of FFRs, such as FFP1, FFP2, and FFP3, minimum filtration efficiencies of 80%, 94%, and 99% can be achieved, respectively [5].

Taking into account the class of the FFRs some differences in the mask construction, especially in
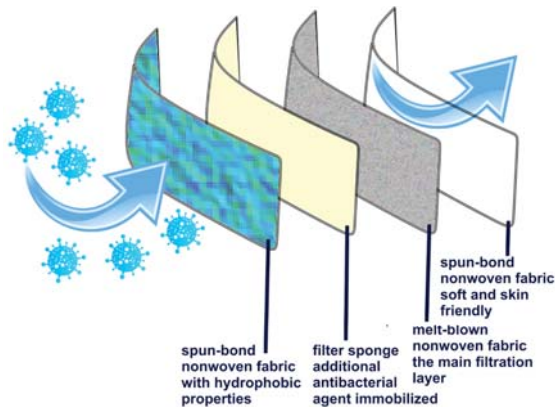
Fig. 1. Schematic of FFR showing different filtration layers.

the number of filtration layers can be observed. Masks meeting FFP1 standards usually are composed of three layers, whereas more than three layers constitute masks that fulfill FFP3 standards. The FFRs are mainly made of non-woven fibrous materials such as polypropylene (PP) [6]. External and internal mask' layers are made of spun-bond PP fabric (Fig. 1). The PP fabric can be electrostatically charged to improve the effectiveness of the filtration without an increase in the flow resistance [7]. Spun-bond non-woven fabrics are composed of continuous filaments produced by an integrated fiber spinning, web formation, and bonding process carried out by thermal, chemical, or mechanical methods and are characterized by high thermal and mechanical resistance and good breathability [8, 9]. The main filtration layer in each FFR is made of non-woven melt-blown PP fabric [10]. In the melt-blown process hot air converges with the fiber as it emerges from the die, whereas in the spun-bond process the hot air flow is at a cross-flow to the emerging fiber [11].

Therefore, the microfibers produced in melt--blown are much finer and the pore size of the non-woven fabric is much smaller [12]. FFRs may contain also additional layers produced from PP modified with activated carbon or silver to enhance its antitoxic or antimicrobial properties [13, 14].

The transport of the aerosol particles carried by the gas stream into the non-woven structure is very complex. The particle deposition on the fiber may occur due to various deposition mechanisms, such as inertia, direct impaction, sedimentation, and diffusion (Brownian motions), and results in electrostatic interactions [15, 16]. For the range of particle diameters, in which none of the above-mentioned mechanisms is dominant, it can be observed minimum in overall filtration efficiency, the so-called most penetrating particle size (MPPS), which is commonly about 0.3 μm. The scheme of the above-mentioned mechanisms together with the scopes of their domination is presented in Fig. 2. For particles and droplets with a diameter 0.3 μm or greater the main dominant mechanisms are interceptions and inertial impaction.

For submicron particles with a diameter 0.3 μm the main mechanisms are diffusion and electrostatic attraction. As a result of collisions with air molecules, aerosol particles undergo a diffusion process, which is manifested as the so-called Brownian motion, which is stochastic and changes in the posi-
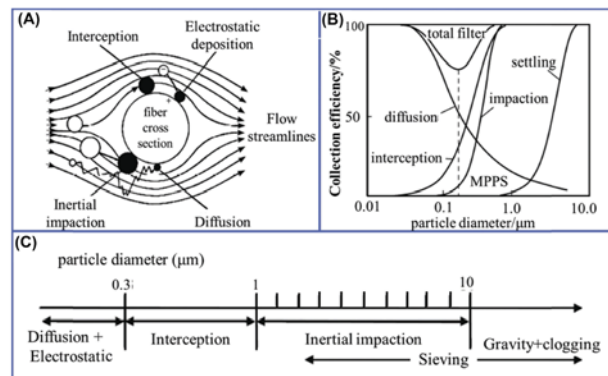

Fig. 2. The scheme of main particles deposition mechanisms on fiber material (A), diagram of the relationship between the filtration efficiency and the particle diameter for a given deposition mechanism; MPPS (B), the main filtration mechanism based on a given range of particle diameters (C). Reproduced with permission [17] Copyright © 2019 Elsevier Inc.

tion of a particle. The importance of the diffusion mechanism is increasing with decreasing the particle diameter and becomes less as the aerosol particle size increases. It is similar to the electrostatic particle deposition mechanism [18–21].

Generally, most PPE is designed to be used only one time and by one person prior to disposal, and should not be reprocessed and reused. However, the outbreak of the COVID-19 pandemic has shown clearly that the current global stockpile of PPE is insufficient, particularly for medical masks and respirators. Moreover, the capacity to expand PPE production is limited therefore, the current demand for respirators and masks cannot be met and the shortages of PPE have become a global problem. Based on current evidence, in consultation with international experts the World Health Organization (WHO) carefully considered the possibility of the reprocessing and reuse of the PPE [22]. However, reprocessing should not affect the integrity of the filtration materials, and respirators after decontamination should still fulfil strict requirements concerning filtration effectiveness. Different methods such as hydrogen peroxide sterilization, ethylene oxide fumigation, UV, microwave oven irradiation, or hot water heating were tested for decontamination of FFRs [22–25]. Recently, different disinfection methods have been extensively studied as a tool for microbiological decontamination of different commercially available FFRs [26]. However, it was simultaneously proved that autoclaving or high-heat (>90°) cannot be used for facepiece respirator treatments because the reduction of filter efficiency in some mask types was observed. Also, physical degradation may be an issue for certain mask models [27].

Ionizing radiation has been widely used for the sterilization of disposable medical products for many years [28]. Due to the high dose rate of EB irradiation, the decontamination of PPE is a very fast process and appropriate dose is delivered within several seconds which could limit post-oxidation--related effects due to the degradation of the materials (polymers) that were used to PPE production [29].

It was confirmed that ionizing radiation is very effective in coronaviruses elimination and dose D_{10} does not exceed 2 kGy [30, 31]. The D_{10} value is the dose required to reduce an exposed microbial population by 90% (one $\log_{10}$) under given conditions.

In this work, three different FFRs (two conforming to the FFP1 standard and one conforming to the FFP3 standard) were irradiated with an electron beam of different doses. Then the effect of EB irradiation on filtration efficiency, morphology, wettability, and thermal and mechanical resistance was determined.

Materials and methods

To compare the influence of EB irradiation on different respirators three different PP masks: popular surgical mask, 3M 1863+ mask conforming to the high FFP3 standard and 3M 9101E mask conforming to the FFP1 standard were chosen for the investigation. Masks were sealed in paper envelopes and irradiated with doses of 12 kGy and 25 kGy in the air atmosphere, at ambient temperature. Electron beam irradiation of samples was carried out using 10 MeV, 10 kW linear electron accelerator 'Elektronika'. Delivered doses were confirmed using a B3 radiochromic foil dosimeter measured with a flat bed scanner and RisoScan software, with uncertainties evaluated at 8%. For all tested samples the dose increase inside the samples was below 1%.

Doses were selected taking into account the assumption of the possible variability in viral load in used masks and its random distribution among products. On the base of microbial contamination found in surgical masks, one can realise that the standard deviation (SD) of the bioburden is higher than the mean N: 47 ± 56 cfu/ml/piece for the inside mask area and 166 ± 199 cfu/ml/piece from mask outside area [31]. This results from the variability of environments where masks are used and differences in the level of the bioburden. On the base of the maximum of 1000 microorganisms that should be present in the product, the decontamination dose (a dose required for 5 or 6 order of magnitude reduction of bioburden) was calculated as 12 kGy [32]. Moreover, masks were also irradiated with a standard sterilization dose of 25 kGy which is defined as sterilization dose according to VD_{max} method given in ISO 11137-2 standard [33]. Masks that were not irradiated were used as control samples.

SEM images of the mask's layers were obtained, using a Hitachi TM-100 scanning electron microscope with an accelerating voltage of 15.0 kV. Samples for the SEM examination were prepared according to a standard procedure, fixed with conductive glue, and coated with a thin layer of gold. The samples were examined at a magnification of 500×.

Thermogravimetric analysis (TGA) of masks samples was used to determine the thermal stability and possible degradation of respirators materials was conducted with a Q500 TGA (TA Instruments, USA) thermogravimetric analyzer in the temperature range 30–600°C at a heating rate of 10°C per minute, under a constant flow (60 mL/min) of nitrogen gas.

Measurements of tensile strain were carried out using an INSTRON 5565 electromechanical universal test machine according to the appropriate standard [34]. Ten measurements of each sample were taken in order to determine the mean values of the tensile strength with high precision. However, values obtained for the test specimen slipped in the jaws, broke within the clamping area, or showed evidence of uneven stretching across its width were rejected.

Dynamic contact angle vs. water was measured using Tensiometer K100C (KRÜSS GmbH, Germany) supplied with the thermostatic sample vessel at 25°C. Applying Wilhelmy method, twenty measurements for each sample were performed and the average value together with standard deviation (SD) was calculated for each sample.

To determine the initial separation efficiency of the tested respirators samples before and after irradiation, the high-quality test bench MFP NanoPlus (Palas GmbH, Germany) was used. The scheme of MFP nanoPlus is presented in Fig. 3.

Fractional and overall filtration effectiveness was determined for solid particles (KCl nanocrystals) as well as oil nanodroplets of Di-Ethyl-Hexyl-Sebacat (DEHS). For tests, circular samples with a diameter of 60 mm were punched from tested respirators. All filtration tests were performed at the airflow rate 95 L/min and the air face velocity of 0.559 m/s. For these experiments, it was required to perform experiments in a sequence of measurements without (upstream) and with (downstream) a filtrating material in the tested chamber. One series consisted of two upstream measurements and two downstream measurements. There were carried out two series of measurements for each mask material. Next, the average value of the filtration effectiveness was calculated and presented in the diagrams below. The time of a single measurement of upstream and downstream was always 380 s. For this time, the interval between measurements was included and it was 60 s. Such a long time of a single measure-
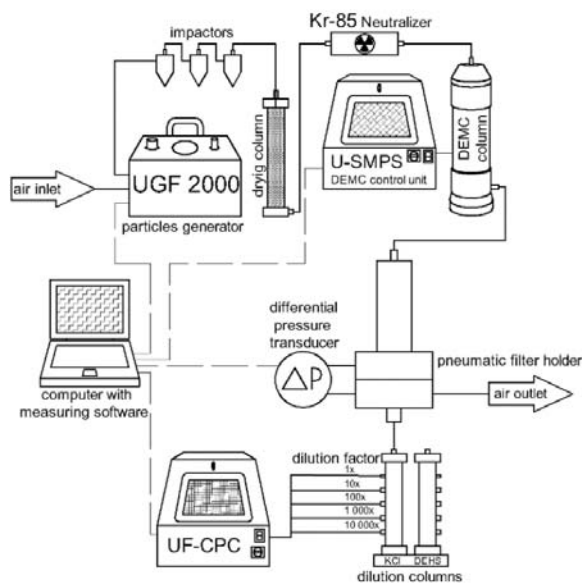

Fig. 3. Scheme of the MFP nanoPlus – test bench for nanoparticle filtration. Reproduced with permission [35] Copyright © Taiwan Association for Aerosol Research.
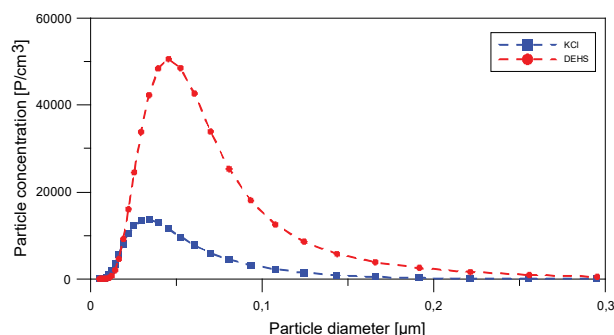
Fig. 4. The particle distribution of aerosol generated by the UGF 2000.

ment was necessary to correctly classify and count nanoparticles. Moreover, during the tests, there were also determined the pressure drops across the tested materials and their initial overall filtration efficiency. The size distribution of the generated aerosols used in the experiments is presented in Fig. 4.

Results and discussion

To visualize different respirators structure the SEM images of the separate layers that compose the Aura (catalog number 1863+), VFlex (catalog number 9101E), and surgical respirators are presented in Figs. 5–7, respectively.

Filtration material used in all tested respirators was composed of pure PP, however, investigation of the Aura respirator filtration fabric revealed that the mask consists of four layers, each of them is composed of the PP fibers of different diameters woven in different packing density (Fig. 5). External and internal mask' layers are made of spun-bond PP fabric. The external layer is composed of uniform fibers with the same diameter of ~20 μm, whereas the internal layer consists of fibers with different diameters in the range of 5–10 μm. The main filtration layer (layer 3)
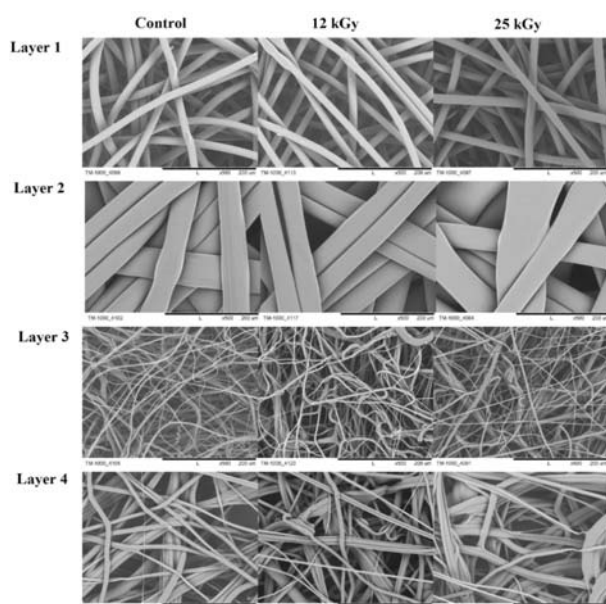

Fig. 5. SEM images of the separate layers of Aura respirators before and after irradiation with electron beam (magnification 500×).

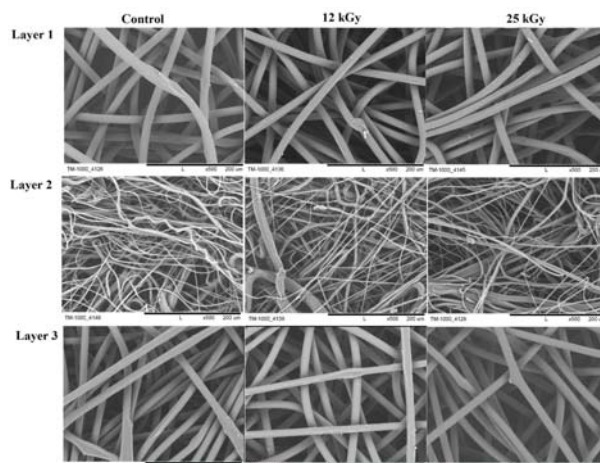**Fig. 6.** SEM images of the separate layers of VFlex respirators before and after irradiation with electron beam (magnification 500×).

is made of non-woven melt-blown PP fabric, which is characterized by very small diameters of the fibers. The size of the fibers composing this layer is in the range of 1–10 μm. Moreover, there is an additional layer (layer 2) in this mask: the filter sponge, which is produced from the fibers with significantly higher dimension (40–80 μm).

Filtration media that composes 9101E respirator consists of three layers, the external and internal fabric seem to be built of the fibers of similar diameter and packing density, while the middle layer is composed of the fibers of significantly smaller diameters. Spun-bond PP fibers of similar diameter (~20 μm) and packing density, while the middle layer is composed of the melt-blown PP fibers of significantly smaller diameters in the range of 1–10 μm (Fig. 6).

Filtration media that composes surgical respirator also consists of three layers. External and internal fabric have similar diameters (in the range of 20–25 μm) and similar packing densities of the fibers. In this case, the middle layer is also composed of the fibers of significantly smaller diameters (~2 μm) (Fig. 7).

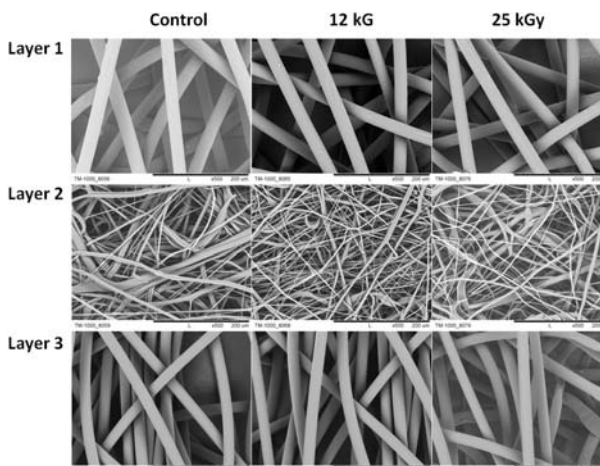All mask layers together were investigated in the presented experiments to determine the overall

Fig. 7. SEM images of the separate layers of surgical respirators before and after irradiation with electron beam (magnification 500×).

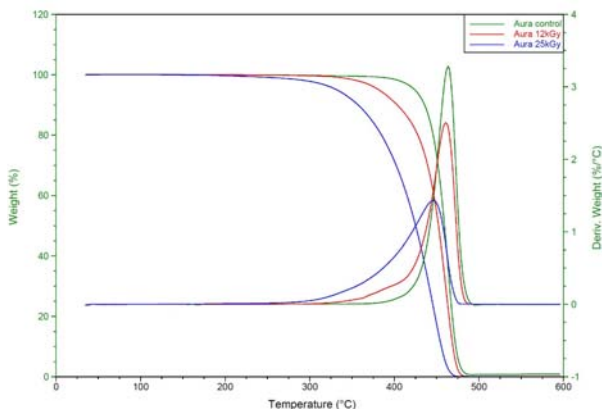**Fig. 8.** Thermograms of Aura respirators irradiated with different doses.

Fig. 10. Thermograms of surgical respirators irradiated with different doses.

properties of the different FFRs after EB irradiation. Any holes or cracks in the structure of the fiber are not visible therefore one can conclude that applied irradiation doses do not affect the morphology of the fibers used for the production of respirators.

Furthermore, the investigation of the thermal properties of respirators irradiated with different EB doses was carried out to determine the influence of radiation on thermal stability. Filtration materials can undergo degradation or cross-linking under irradiation. Thermal decomposition of the material of all samples is a single-step process with one peak in temperature ~445–460°C which is characteristic of PP degradation [36]. PP decomposes into a large number of aliphatic compounds without a residue [37].

In the case of the Aura respirator, visible degradation of the material was confirmed (Fig. 8). The higher the irradiation dose is the more visible the drop in the recorded onset temperature. The onset temperature is 443°C for the control sample, whereas a drop of about 60°C in the onset temperature is observed for the sample irradiated with the dose of 25 kGy. Moreover, a significant drop in temperatures of the maximum in the loss weight rate with the irradiation dose increase can be also observed.

In the case of the VFlex respirator, similar degradation of the material for both irradiation doses was observed (Fig. 9). The onset temperature is 396°C for the control sample, whereas a drop of about 30°C in the onset temperature is observed for the samples irradiated with the dose of 12 kGy and 25 kGy. In
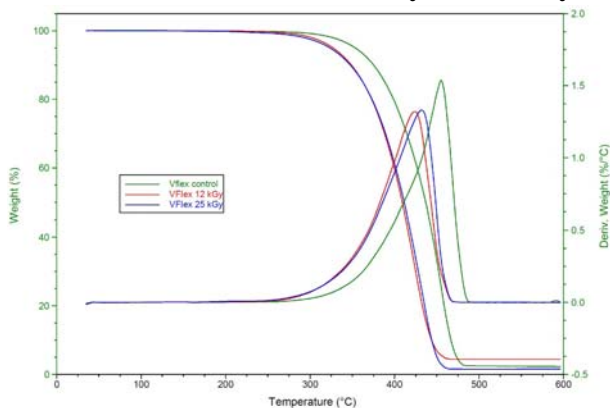
this case, a similar decrease of temperatures of the maximum in the loss weight rate for both irradiation doses is observed.

The smallest drop in onset temperature is observed for the irradiated surgical respirators (Fig. 10). The onset temperature is 445°C for the control sample, whereas a drop of about 20°C in the onset temperature is observed for the samples irradiated with the dose of 12 kGy and 25 kGy. Therefore, one can conclude that the irradiation even with the lowest required dose influences the thermal properties of all studied types of FFRs.

In the next step, the investigation of the mechanical properties of respirators irradiated with different EB doses was carried out to determine the influence of radiation on the mechanical resistance of the fabrics. Changes in tensile strain for different kinds of FFRs irradiated with different doses are shown in Figs. 11A–11C, respectively. It is visible that tearing of the fabrics that compose Aura and VFlex mask is single-stage process in which all the layers are torn off simultaneously, whereas two-stage process consists of tearing off second and internal layer primary followed by tearing of external layer is observed for the surgical mask (Fig. 11). Average values of tensile strength together with SDs for each FFR before and after irradiation are presented in Table 1. No significant changes in tensile strength were observed even for the masks irradiated with a dose 25 kGy.

Contact angle studies provide information on the wettability of masks' materials. Contact angles measured for each mask before and after irradiation are presented together with SD of the measurements are presented in Fig. 12.

Very small differences in measured contact angles for non-irradiated and irradiated samples of all FFRs indicate that even irradiation with the dose of 25 kGy does not affect surface hydrophobicity. Hydrophobic properties of the surface are observed for all types of FFRs before and after EB irradiation. A small decrease in the value of contact angle can be related to the elimination of some of the electric charges from the surface of investigated material after the irradiation procedure [38, 39].

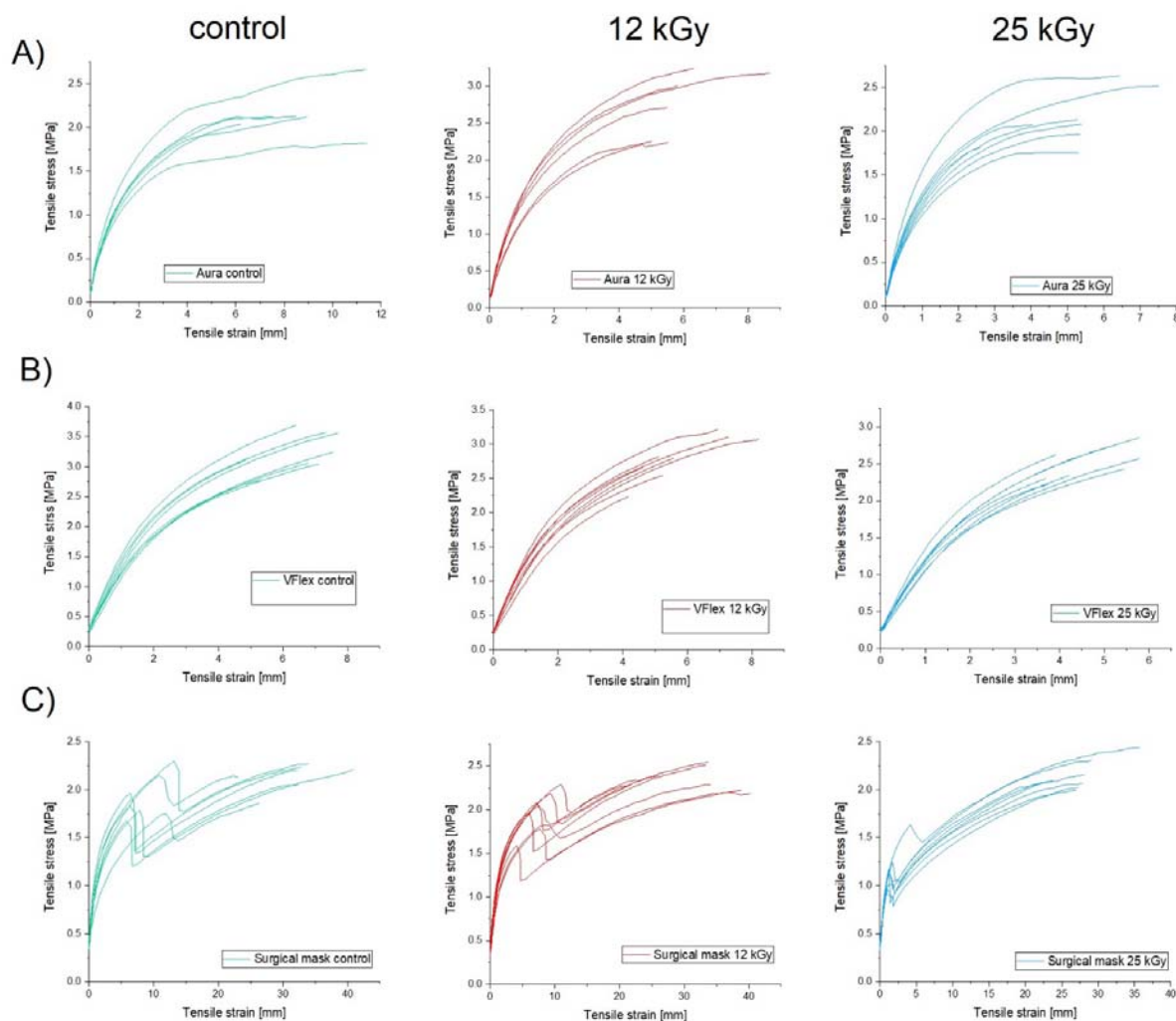It was observed that there was a decrease in filtration efficiency for irradiated respirators in

Fig. 9. Thermograms of VFlex respirators irradiated with different doses.

Fig. 11. Changes of tensile strain for Aura mask (A), VFlex mask (B), and surgical masks (C) for different irradiation doses.

Table 1. Average values of tensile strength together with SDs for all studied FFRs before and after irradiation

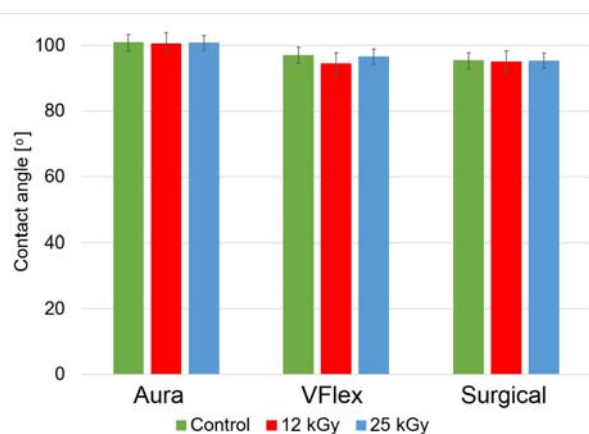| Mask type	Aura		VFlex		Surgical	
Dose (kGy)	Tensile strength (MPa)	SD	Tensile strength (MPa)	SD	Tensile strength (MPa)	SD
0 (control)	1.91	0.14	3.17	0.34	2.20	0.16
12	2.35	0.66	2.78	0.33	2.21	0.32
25	2.05	0.32	2.51	0.20	2.07	0.22

Fig. 12. Water contact angle values for FFRs before and after EB irradiation.

comparison to the control samples. The decrease in filtration efficiency observed for respirators irradiated with both doses was similar. Moreover, for both respirators, it was observed that filtration efficiency decreased with the increase of the particle diameter (Fig. 13).

The main mechanical mechanism of deposition for nanoparticles is diffusion (Brownian motion). When the particle diameter increases, the Brownian motion is less intense, thus diffusional mechanism becomes less important in the process of particle deposition, which explains the observed phenomenon.

A decrease in filtration efficiency may result from the elimination of the electric charge from the PP fibers in the irradiation process. To support this theory conditioning of the non-irradiated samples
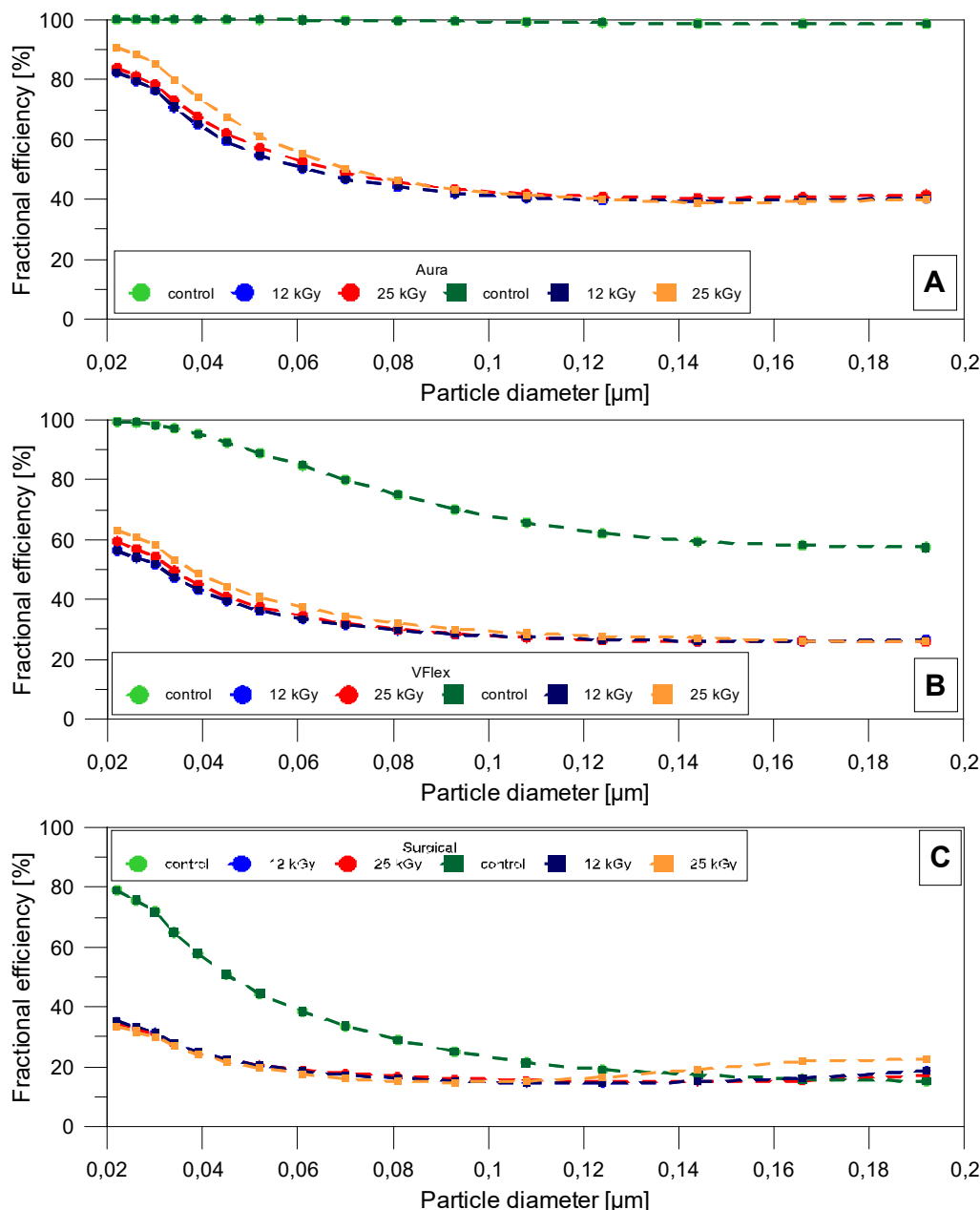
Fig. 13. Fractional efficiency of removal KCl and DEHS particles for Aura (A), VFlex (B), and surgical (C) respirators before and after irradiation with EB.

of respirators in isopropanol (IPA) vapours was applied to remove the electric charge from the surface of studied filtrating materials [40]. Obtained results confirmed that the drop in filtration efficiency for the irradiated filters is connected with the elimination of the electric charge from the fiber surface (Fig. 14).

Baseline filtration efficiency was very high for both respirators: 99.7% for Aura respirator and 90.2% for VFlex respirator, whereas after irradiation with both doses filtration efficiency dropped to 62% (average value for droplets and particles filtration) for respirator Aura irradiated with 12 kGy and similarly, a value of 66% was obtained for this respirator irradiated with 25 kGy. Even more significant decrease in filtration efficiency to 42% for respirators irradiated with 12 kGy and 44% for masks irradiated with 25 kGy was observed for Flex respirators (Fig. 15).

In the case of a surgical mask, a similar observation can be made (see Fig. 16). The average filtration efficiency control mask reached 55.2%, while after EB irradiation the overall efficiency decreased to 27.1% and 24.8% for 12 kGy and 25 kGy, respectively.

The decrease in filtration efficiency observed for control samples conditioned in IPA was similar to the drop in filtration efficiency determined for irradiated samples which supports the theory that irradiation eliminates electric charge from the surface of PP fibers. Moreover, filtration efficiency observed for irradiated samples conditioned additionally in IPA remained almost at the same level (see Fig. 17).

Additionally, pressure drop across the filtrating materials was determined for each respirator to investigate the influence of the irradiation on the integrity and stability of the filtration materials (Fig. 18).
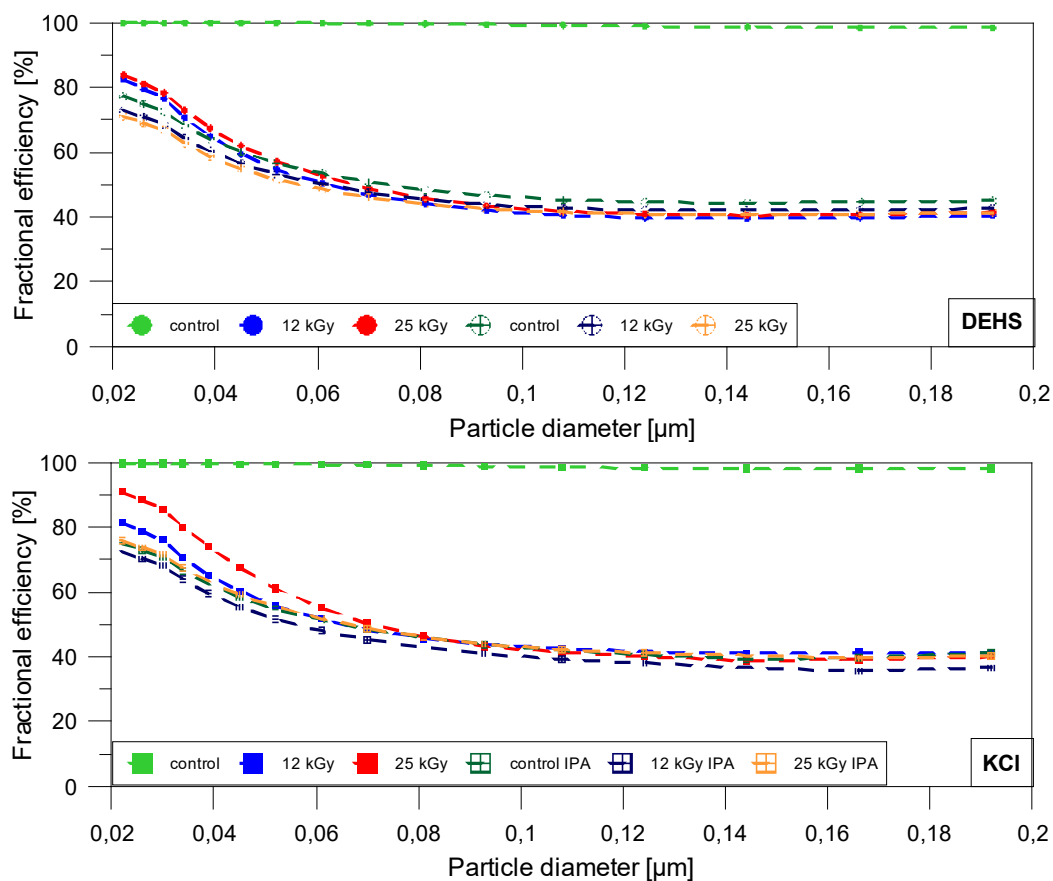
Fig. 14. Fractional efficiency of removal DEHS and KCl particles for Aura respirators after conditioning in IPA vapours.
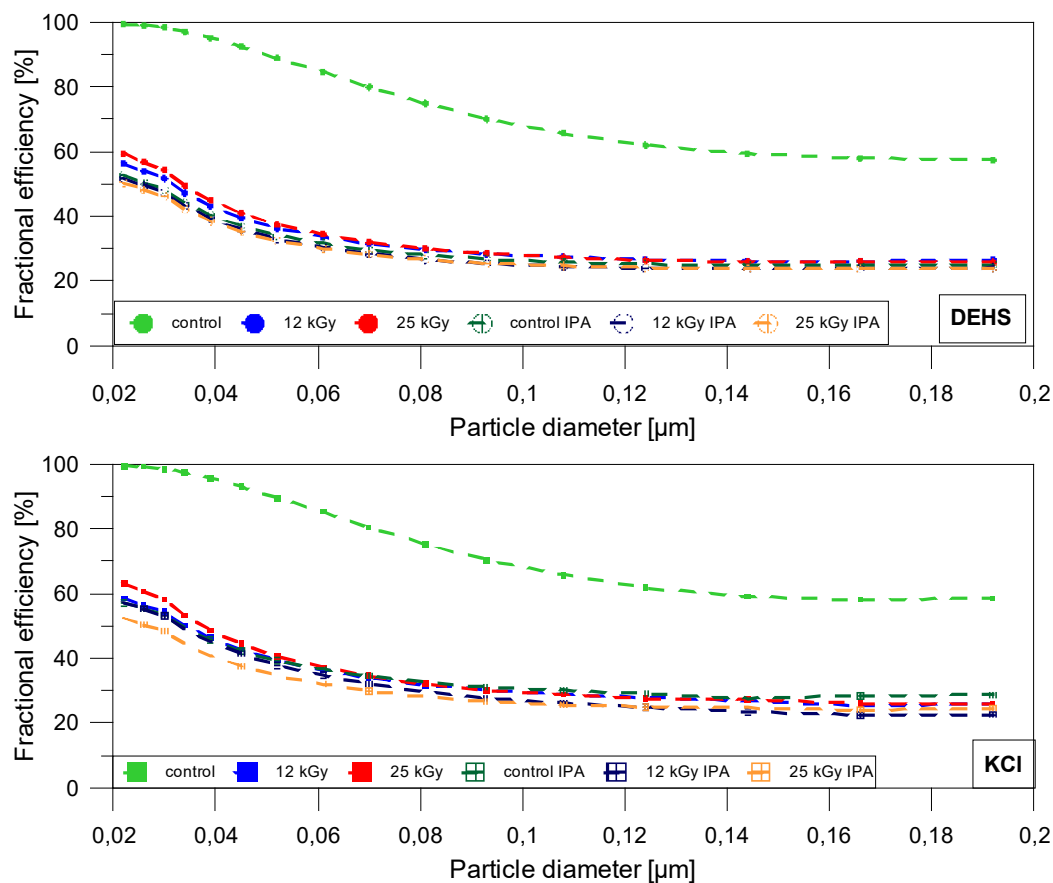

Fig. 15. Fractional efficiency of removal of DEHS and KCl particles for VFlex respirators after conditioning in IPA vapours.
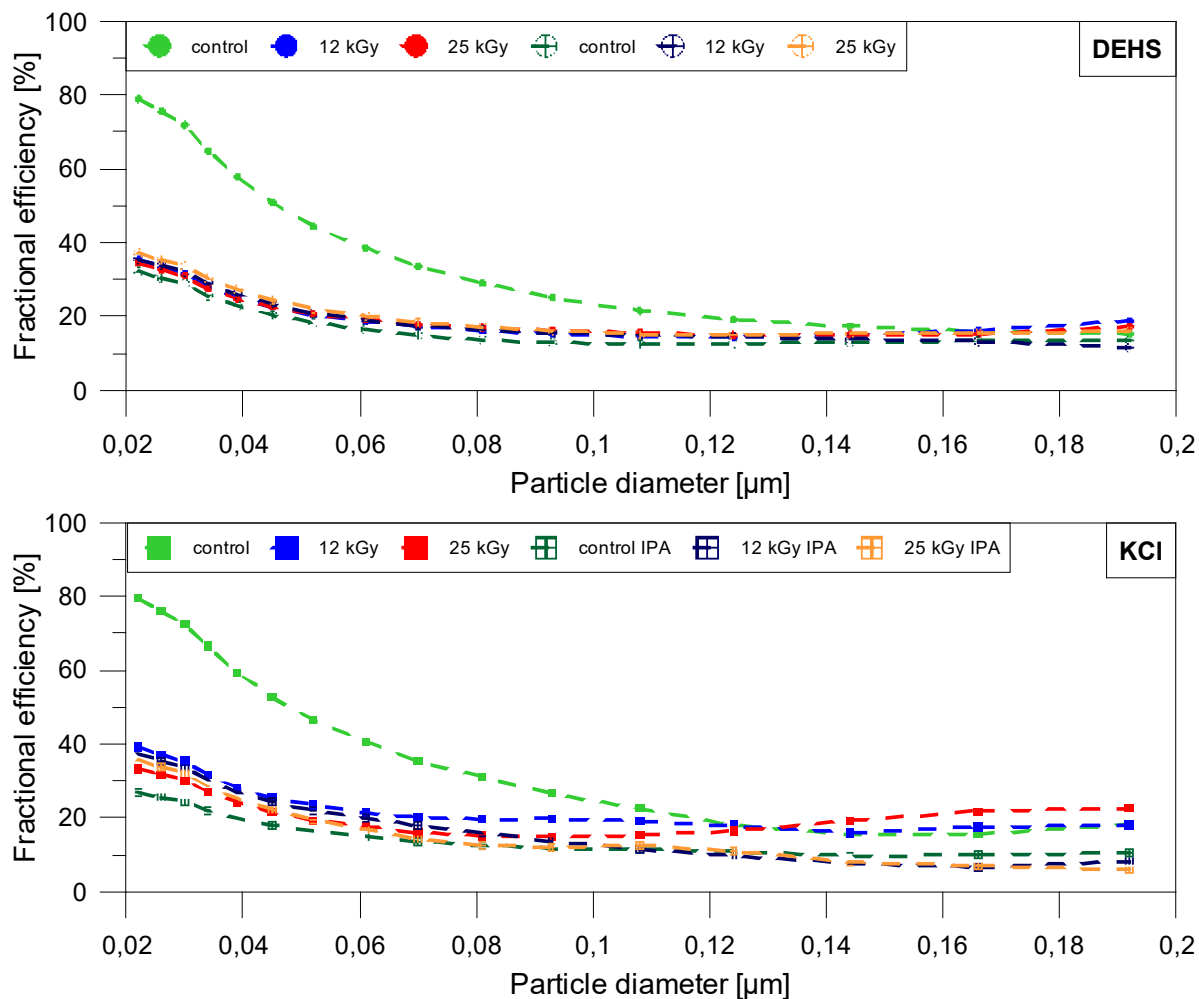
Fig. 16. Fractional efficiency of removal DEHS and KCl particles for surgical mask after conditioning in IPA vapours.
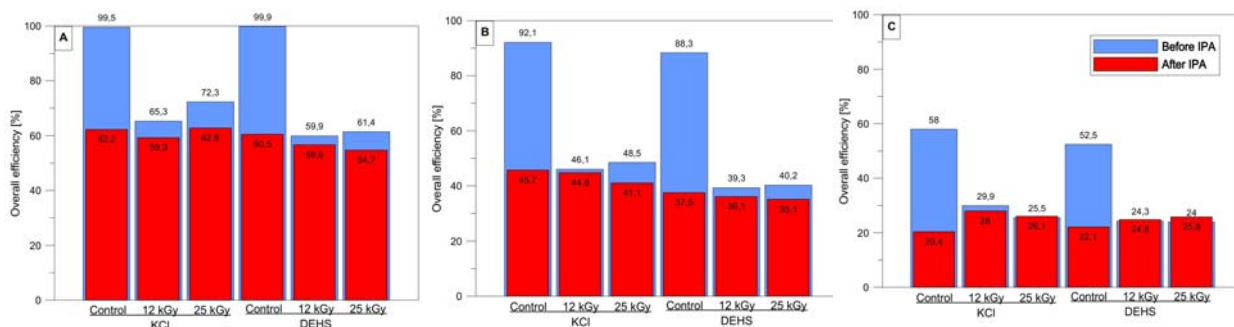

Fig. 17. Comparison of overall filtration efficiency of removal KCl and DEHS particles for Aura (A), VFlex (B), and surgical (C) respirators before and after irradiation and conditioning in IPA vapours.
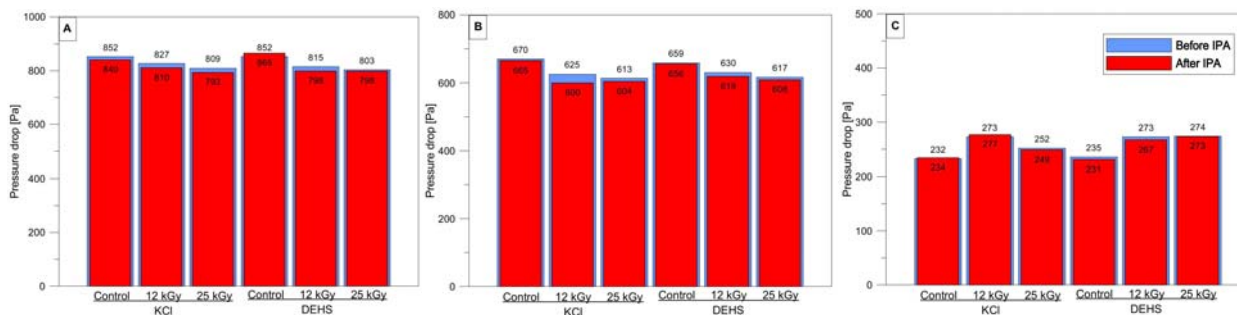

Fig. 18. Pressure drops across the filtrating materials determined for Aura (A), VFlex (B), and surgical (C) respirators before and after irradiation and conditioning in IPA vapours.

In most cases, a small decrease in the pressure drop across the filtrating materials after irradiation was observed for both respirators. However, observed differences in pressure drop for control and irradiated samples were so small that cannot be connected with the changes in the structure of the filtrating material.

Conclusions

Irradiation of three different FFRs with EB irradiation allows to determine that applied irradiation doses may affect filtrating materials' stability and integrity. SEM analysis revealed that the morphology of the fibers used for the respirators production remains the same after irradiation with both doses as the morphology of control samples and any effect like cracks and holes are not visible for all filtrating layers. Mechanical properties and wettability of the irradiated PP fabrics composed of all studied FFRs did not change even after irradiation with the dose of 25 kGy. However, one should bear in mind that the post-irradiation oxidative effects that are observed for PP samples may deteriorate the mechanical properties of studied fabrics in time after irradiation. Moreover, a significant change in thermal stability of all FFRs is observed for all irradiated samples.

The results presented confirmed that the decrease in filtration efficiency after irradiation of both respirators results from the elimination of the electric charge from the PP fibers in the irradiation process. Therefore, decontamination of FFRs with EB irradiation is problematic without regard to applied doses. Nevertheless, applied doses did not influence filtering materials' structure and integrity, and therefore the application of the treated masks in this way can be considered after the restoration of electric charge which is crucial for their filtering function.

ORCID

D. Chmielewska http://orcid.org/0000-0002-4806-1000
U. Gryczka http://orcid.org/0000-0003-2221-4176
W. Migdał http://orcid.org/0000-0003-3382-376X
Ł. Werner http://orcid.org/0000-0003-3492-2364

References

1. Yu, I. T. S., Li, Y., Wong, T. W., Tam, W., Chan, A. T., Lee, J. H. W., Leung, D. Y. C., & Ho, T. (2004). Evidence of airborne transmission of the severe acute respiratory syndrome virus. *N. Engl. J. Med.*, *350*, 1731–1739. DOI: 10.1056/nejmoa032867.

2. Neeltje van Doremalen, V. J. M., Bushmaker, T., Morris, D. H., Holbrook, M. G., Gamble, A., Williamson, B. N., Tamin, A., Harcourt, J. L., Thornburg, N. J., Gerber, S. I., Lloyd-Smith, J. O., & de Wit, E. (2020). Aerosol and surface stability of SARS-CoV-2 as compared with SARS-CoV-1. *N. Engl. J. Med.*, *382*, 1564–1567. DOI: 10.1056/NEJMc2004973.

3. Morawska, L., & Cao, J. (2020). Airborne transmission of SARS-CoV-2: The world should face the reality. *Environ. Int.*, *139*, 105730. DOI: 10.1016/j.envint.2020.105730.

4. Morawska, L., Johnson, G. R., Ristovski, Z. D., Hargreaves, M., Mengersen, K., Corbett, S., Chao, C. Y. H., Katoshevski, Y., & Li, D. (2009). Size distribution and sites of origin of droplets expelled from the human respiratory tract during expiratory activities. *J. Aerosol Sci.*, *40*, 256–269. DOI: 10.1016/j.jaerosci.2008.11.002.

5. The Polish Committee for Standardization. (2010). Respiratory protective devices. Filtering half masks to protect against particles. Requirements, testing, marking. PN-EN 149+A1:2010 (in Polish).

6. Dowd, K. O., Nair, K. M., Forouzandeh, P, Mathew, S., Grant, J., Moran, R., Bartlett, J., Bird, J., & Pillai, S. C. (2020). Face masks and respirators in the fight against the COVID-19 pandemic: A review of current materials, advances and future perspectives. *Materials*, *13*(2), 3363. DOI: 10.3390/ma13153363.

7. Zhang, H., Liu, J., Zhang, X., Huang, C., & Jin, X. (2018). Design of electret polypropylene melt blown air filtration material containing nucleating agent for effective PM2.5 capture. *RSC Adv.*, *8*, 7932–7941. DOI: 10.1039/c7ra10916d.

8. Midha, V. K., & Dakuri, A. (2017). Spun bonding technology and fabric properties: A review. *J. Text. Eng. Fash. Technol.*, *1*, 126–133. DOI: 10.15406/jteft.2017.01.00023.

9. Agarwal, S., Wendorff, J. H., & Greiner, A. (2008). Use of electrospinning technique for biomedical applications. *Polymer (Guildf)*, *49*, 5603–5621. DOI: 10.1016/j.polymer.2008.09.014.

10. Pandey, L. K., Singh, V. V., Sharma, P. K., Meher, D., Biswas, U., Sathe, M., Ganesan, K., Thakare, V. B., & Agarwal, K. (2021). Screening of core filter layer for the development of respiratory mask to combat COVID-19. *Sci. Rep.*, *11*, 1–14. DOI: 10.1038/s41598-021-89503-x.

11. Hutten, I. M. (2007). Processes for nonwoven filter media. In *Handbook of nonwoven filter media*. (Chapter 5, pp. 195–244). Oxford: Butterworth-Heinemann.

12. Chua, M. H., Cheng, W., Goh, S. S., Kong, J., Li, B., Lim, J. Y. C., Mao, L., Wang, S., Xue, K., Yang, L., Ye, E., Zhang, K., Cheong, W. C. D., Tan, B. H., Li, Z., Tan, B. H., & Loh, X. J. (2020). Face masks in the new COVID-19 normal: Materials, testing, and perspectives. *Research (Wash DC)*, *2020*, 1–40. DOI: 10.34133/2020/7286735.

13. Khayan, K., Anwar, T., Wardoyo, S., & Puspita, W. L. (2019). Active carbon respiratory masks as the adsorbent of toxic gases in ambient air. *J. Toxicol.*, *2019*, 5283971. DOI: 0.1155/2019/5283971.

14. Fouad, G. I. (2021). A proposed insight into the anti-viral potential of metallic nanoparticles against novel coronavirus disease-19 (COVID-19). *Bull. Natl. Res. Cent.*, *45*(1), 36. DOI: 10.1186/s42269-021-00487-0.

15. Hinds, W. C. (1999). *Aerosol technology: properties, behavior, and measurement of airborne particles.* Los Angeles: Wiley.

16. Brown, R. C. (1993). *Air filtration: an integrated approach to the theory and applications of fibrous filters.* Oxford; New York: Pergamon Press.

17. Zhang, S., Rind, N. A., Tang, N., Liu, H., Yin, X., Yu, J., & Ding, B. (2019). Electrospun nanofibers for air filtration. In B. Ding, X. Wang & J. Yu (Eds.), *Electrospinning nanofabrication application* (pp. 365–389). William Andrew Publishing.

18. Choi, D. Y., An, E. J., Jung, S. H., Song, D. K., Oh, Y. S., Lee, H. W., & Lee, H. M. (2018). Al-coated conductive fiber filters for high-efficiency electrostatic filtration: Effects of electrical and fiber structural properties. *Sci. Rep.*, *8*, 1–10. DOI: 10.1038/s41598-018-23960-9.

19. Wang, C. S. (2001). Electrostatic forces in fibrous filters – A review. *Powder Technol.*, *118*, 166–170. DOI: 10.1016/S0032-5910(01)00307-2.

20. Oh, Y. W., Jeon, K. J., Jung, A. Y., & Jung, Y. W. (2002). A simulation study on the collection of submicron particles in a unipolar charged fiber. *Aerosol Sci. Technol.*, *36*, 573–582. DOI: 10.1080/02786820252883810.

21. Yang, S., & Lee, G. W. M. (2005). Filtration characteristics of a fibrous filter pretreated with anionic surfactants for monodisperse solid aerosols. *J. Aerosol Sci.*, *36*, 419–437. DOI: 10.1016/j.jaerosci.2004.10.002.

22. Schwartz, A., Stiegel, M., Greeson, N., Vogel, A., Thomann, W., Brown, M., Sempowski, G. D., Alderman, T. S., Condreay, J. P., Burch, J., Wolfe, C., Smith, B., & Lewis, S. (2020). Decontamination and reuse of N95 respirators with hydrogen peroxide vapor to address worldwide personal protective equipment shortages during the SARS-CoV-2 (COVID-19) pandemic. *Appl. Biosaf.*, *25*, 67–70. DOI: 10.1177/1535676020919932.

23. Viscusi, D. J., Bergman, M. S., Eimer, B. C., & Shaffer, R. E. (2009). Evaluation of five decontamination methods for filtering facepiece respirators. *Ann. Occup. Hyg.*, *53*, 815–827. DOI: 10.1093/annhyg/mep070.

24. Mackenzie, D. (2020). Reuse of N95 masks. *Engineering (Beijing)*, *6*, 593–596. DOI: 10.1016/j.eng.2020.04.003.

25. Lindsley, W. G., Martin, S. B., Thewlis, R. E., Sarkisian, K., Nwoko, J. O., Mead, K. R., & Noti, J. D. (2015) Effects of ultraviolet germicidal irradiation (UVGI) on N95 respirator filtration performance and structural integrity. *J. Occup. Environ. Hyg.*, *12*, 509–517. DOI: 10.1080/15459624.2015.1018518.

26. Derraik, J. G. B., Anderson, W. A., Connelly, E. A., & Anderson, Y. C. (2020). Rapid review of SARS-CoV-1 and SARS-CoV-2 viability, susceptibility to treatment, and the disinfection and reuse of ppe, particularly filtering facepiece respirators. *Int. J. Environ. Res. Public Health*, *17*, 1–31. DOI: 10.3390/ijerph17176117.

27. Gertsman, S., Agarwal, A., O'Hearn, K., Webster, R., Tsampalieros, A., Barrowman, N., Sampson, M., Sikora, L., Staykov, E., Ng, R., Gibson, J., Dinh, T., Agyei, K., Chamberlain, G., & McNally, J. D. (2020). Microwave- and heat-based decontamination of N95 filtering facepiece respirators: a systematic review. *J. Hosp. Infect.*, *106*, 536–553. DOI: 10.1016/j.jhin.2020.08.016.

28. Chmielewski, A. G. (2007). Practical applications of radiation chemistry. *Russ. J. Phys. Chem. A*, *81*, 1488–1492. DOI: 10.1134/S0036024407090270.

29. Chmielewska-Śmietanko, D., Gryczka, U., Migdał, W., & Kopeć, K. (2018). Electron beam for preservation of biodeteriorated cultural heritage paper-based objects. *Radiat. Phys. Chem.*, *143*, 89–93. DOI: 10.1016/j.radphyschem.2017.07.008.

30. Commonwealth of Australia. (2014). *Gamma irradiation as a treatment to address pathogens of animal biosecurity concern*. Retrieved March 23, 2022, from http://www.agriculture.gov.au/SiteCollectionDocuments/ba/memos/2014/gamma-irradiation-review.pdf.

31. Feldmann, F., Shupert, W. L., Haddock, E., Twardoski, B., & Feldmann, H. (2019). Gamma irradiation as an effective method for inactivation of emerging viral pathogens. *Am. J. Trop. Med. Hyg.*, *100*, 1275–1277. DOI: 10.4269/ajtmh.18-0937.

32. International Atomic Energy Agency. (2020). *Sterilization and reprocessing of personal protective equipment (PPE), including respiratory masks, by ionizing radiation*. Vienna: IAEA. Retrieved November 23, 2021, from http://www-naweb.iaea.org/napc/iachem/working_materials/Technical%20Report%20%28Mask%20Reprocessing%29.pdf.

33. International Organization for Standardization. (2013). Sterilization of health care products – Radiation – Part 2: Establishing the sterilization dose. ISO 11137-2:2013. Switzerland.

34. American Society for Testing and Material. (2019). Standard Test Method for Breaking Force and Elongation of Textile Fabrics (Strip Method). ASTM D5035-11. West Conshohocken, PA.

35. Jackiewicz, A., & Werner, Ł. (2015). Separation of nanoparticles from air using melt-blown filtering media. *Aerosol Air Qual. Res.*, *15*, DOI: 10.4209/aaqr.2015.04.0236.

36. Esmizadeh, E., Tzoganakis, C., & Mekonnen, T. H. (2020). Degradation behaviour of polypropylene during reprocessing and its biocomposites: Thermal and oxidative degradation kinetics. *Polymers (Basel)*, *12*(8), 1627. DOI: 10.3390/POLYM12081627.

37. Bockhorn, H., Hornung, A., Hornung, U., & Schawaller, D. (1999). Kinetic study on the thermal degradation of polypropylene and polyethylene. *J. Anal. Appl. Pyrolysis*, *48*, 93–109. DOI: 10.1016/S0165-2370(98)00131-4.

38. Bormashenko, E., Pogreb, R., Stein, T., Whyman, G., Schiffer, M., & Aurbach, D. (2011). Electrically deformable liquid marbles. *J. Adhes. Sci. Technol.*, *25*, 1371–1377. DOI: 10.1163/016942411×555953.

39. Bormashenko, E., Pogreb, R., Stein, T., Whyman, G., & Hakham-Itzhaq, M. (2009). Electrostatically driven droplets deposited on superhydrophobic surfaces. *Appl. Phys. Lett.*, *95*, 1–3. DOI: 10.1063/1.3276697.

40. International Organization for Standardization. (2016). Air filters for general ventilation – Part 4: Conditioning method to determine the minimum fractional test efficiency. ISO 16890-4:2016. Switzerland.